Lasers in Manufacturing Conference 2021

High-speed synchrotron x-ray imaging of the formation of wedge-shaped capillaries during laser-beam welding at high feed rates

Eveline N. Reinheimer[a,*], Marc Hummel[b], Alexander Olowinsky[c], Rudolf Weber[a], Thomas Graf[a]

[a]*Universität Stuttgart Institut für Strahlwerkzeuge (IFSW), Pfaffenwaldring 43, 70569 Stuttgart, Germany*
[b]*Chair for Laser Technology LLT, RWTH Aachen University, Steinbachstraße 15, 52074 Aachen,Germany*
[c] *Fraunhofer Institute for Laser Technology ILT, Steinbachstraße 15, 52074 Aachen, Germany*

Abstract

In case of high welding velocities, the geometry of the capillary during laser-beam welding elongates in feed direction to a wedge shape. Following to the change of the capillary, the weld pool changes and the melt velocity increases. Therefore, high-speed X-ray imaging to study the time evolution of capillary geometry and weld pool shape during high-speed laser welding was performed at DESY's synchrotron. The investigation addressed the transition of the capillary geometry from a high aspect ratio to a wedge-shape geometry and how the weld pool geometry and the weld flow changed. In order to investigate the melt flow in the weld pool during welding, the movement of tungsten carbide particles was analysed in the acquired image sequences. The tungsten particles were deposited on top of the sample before welding. Further, a simple method to determine the average melt velocity around the capillary without tracking the tungsten particles is shown. A laser spot diameter of 100 µm and feed rates of up to 2 m/s were used to weld in aluminium.

Keywords: Laser High Speed Welding; Capillary; Weld pool; Synchrotron

* Corresponding author. Tel.: +49-711-68569730 .
E-mail address: Eveline-nicole.reinheimer@ifsw.uni-stuttgart.de

1. Introduction

Investigations, as of Kouraytem et al., 2019, Fetzer et al., 2021 and Hagenlocher et al., 2018 in high-speed laser welding showed that for increasing feed rates the capillary elongates in feed direction. Fabbro, 2010 demonstrated that also the weld pool dynamics changes over the feed rate and that high melt flow velocities advantage weld defects such as humping and undercuts. So far, the melt velocity cannot be measured directly. Therefore, this investigation was performed at the X-ray beamline Petra III at DESY to measure the change of the capillary and the change of the corresponding weld pool in aluminum Al99.5. The melt flow inside the sample was visualized with tungsten tracer particles. The observed capillary geometries and weld pool shapes were used to determine the average melt velocity around the capillary. A method to determine the average melt velocity around the capillary is presented.

2. Method

The experiment at Petra III at DESY (Schell et al., 2013) was carried out in cooperation of the IFSW and the RWTH in Aachen. The detailed experimental set up is described in Lind et al. (submitted to NOLAMP 2021). Figure 1 shows a sketch of the experimental setup. Deep-penetration laser-beam welding in aluminum (Al99.5) was carried out using a TruDisk5000 laser from Trumpf with a wavelength of 1.03 µm. A fiber with a core diameter of 50 µm was used to transport the laser beam to the laser optics with a magnification of 163:80 resulting in a measured spot diameter of 102 µm. The laser beam was focused on the surface of the sample. Welds with feed rates v up to 2 m/s were analyzed with a maximum laser power of P = 5 kW. In the presented pictures, the sheet was moved from right to left while the laser beam was resting with constant position and orientation. Tungsten particles were used to visualize the melt flow. The tungsten particles were placed on top of the sample. The particles had a diameter of 65 µm up to 105 µm. The monochromatic X-ray beam with a photon energy of 37.7 keV and an approximated diameter of 3 mm propagated through the sample in the direction of the *y*-axis. The absorption of the radiation depends on the effective material thickness along the path through the material. The local difference in brightness between the capillary and the remaining material can be used to calculate the remaining thickness of the material. The gray value information of each pixel contains the information about the thickness of the material at the location of the pixel. The transmitted X-ray beam is converted to visible light by a scintillator and was recorded by a HS camera with 1000 frames per second with a high spatial resolution of 256 px/mm.

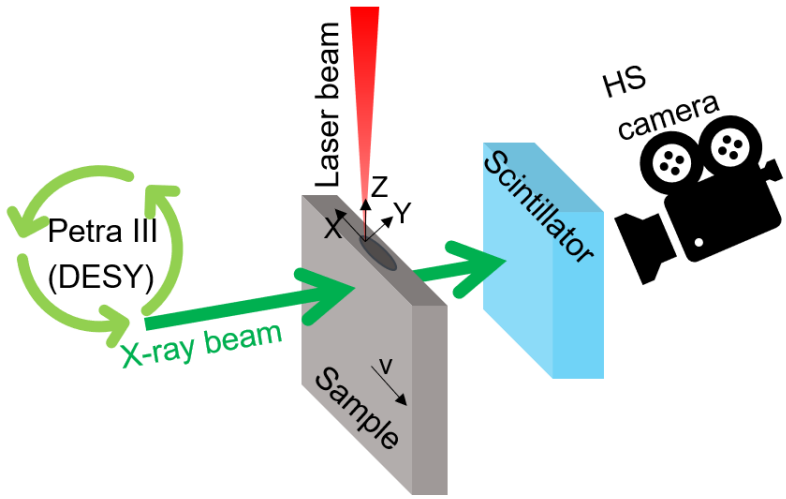

Fig.1. Experimental set up at DESY. The X-ray beam passes through the sample during welding. The scintillator converts the X-ray beam into visible light, which is recorded with a high-speed camera. Described in detail by Lind. et al.

3. Results

Typical images of the X-ray recorded videos of laser beam welding at different feed rates, taken at DESY, can be seen in Fig. 2. In the video, the phase transition from solid to liquid can be seen very well. In the single image, however, the transition is barely visible. This is why the capillary is highlighted with a white dashed line and the weld pool is marked with a dash-dotted line. The numerous black marks in the weld pool are due to tungsten particles, which allow to visualize the melt flow. The welding depth is marked with an arrow and with the corresponding value above the arrow. For a lower feed rate of 0.2 m/s, as shown in the top X-ray image of Fig. 2 a, the capillary geometry is cylindrical, the weld pool shape from the bottom of the capillary to the surface is similar to a quarter circle. The visible tungsten particles in the X-ray video indicate eddies in the weld stream marked by the red arrow in Fig. 2a. By increasing the feed rate to 0.8 m/s (Fig. 2b), it can be seen that the capillary geometry changes to a U-shape. The rear wall of the capillary moves away from the front and opens the capillary. The weld pool is elongated and the shape of the weld pool in the X-ray image changes to a quarter-elliptical shape. There are no eddies visible in the weld-pool, the tracer particles seem to move on a wavelike path from the capillary to the end of the weld pool. By increasing the feed rate even higher, the geometry of the capillary changes to a wedge shape (Fig 2c). The weld-pool depth below the capillary decreases approximately linearly towards the sample surface. It seems that the tracer in the weld pool under the capillary move in a fast “jet” without any eddies, which is clearly visible in the video, but unfortunately due to the noise, only barley visible in the single-frame. The capillary and the weld pool exceed the image border in the lower X-ray image, for this reason no direct statement can be made about the end of the weld pool. The investigation showed that not just the capillary geometry changes over the feed rate, but also the weld-pool shape. For increasing feed rate the weld pool elongates as well and its shape changes from a “quarter circle” to a “wedge shape” in the X-ray image.

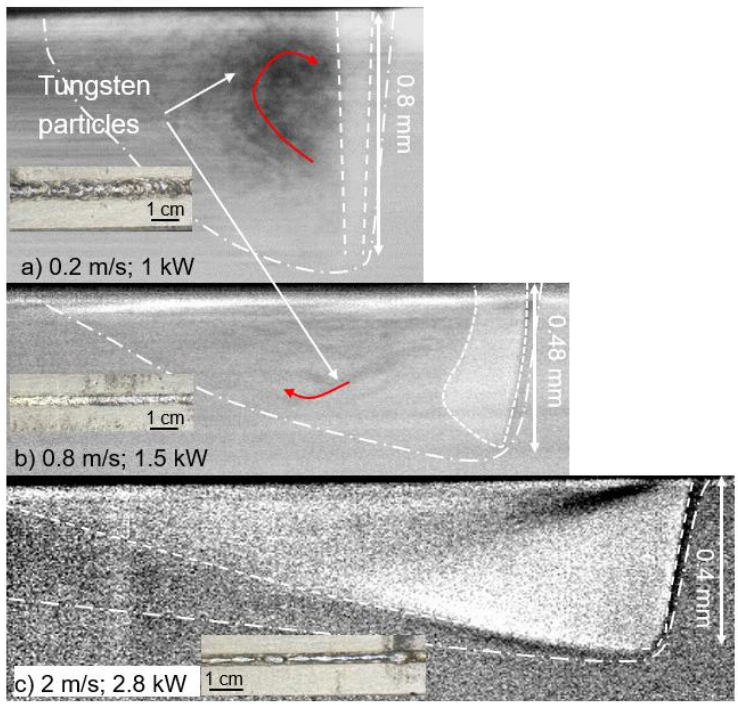

Fig. 2. Images of the recorded X-Ray video of the steady state process for three different feed rates and laser powers.

3.1. Method to determine the average melt velocity

The frame rate of 1000 fps was too low to be able to determine the melt velocity by tracking the tracer particles, especially in case of high melt velocities when a wedge-shaped capillary was formed. However, using cross sections and reconstructed capillaries from the X-ray image (Boley et al., 2013), the average melt velocity $\bar{u}$ around the capillary can be estimated as described in the following. The molten and resolidified area A_{QS} was measured in the cross section (Fig. 3) and the capillary was reconstructed from the X-ray image (Fig. 3). From the reconstructed capillary, the cross-section area of the capillary A_{cap} was determined. In Fig. 3 two positions are indicated at which the average melt velocity was determined. Position 1, where the capillary is the deepest, and position 2 further back are used. For the U-shaped and cylindrical shaped capillaries only position 1, where the capillary is the deepest, was analysed. The cross-section area of the capillary for these two positions was measured. At position 1 the liquid area A_1 is equal to

$$A_1 = A_{QS} - A_{cap,1}, \tag{1}$$

where $A_{cap,1}$ is the determined area of the reconstructed capillary at position1 (Fig. 3, left). At position 2, some material under the capillary and of the side of the weld pool was already resolidified, which was visible in the video by the phase transition of solid to liquid. The amount of the resolidified area under the weld pool can be estimated by the weld pool line at position 2, highlighted in Fig. 3 by the yellow long dashed line. The resolidified material at the side of the weld pool was neglected. The area of the liquid area at position 2 A_2 can be calculated with

$$A_2 = A_{QS} - A_{cap,2} - A_{solid,2} \tag{2}$$

where $A_{cap,2}$ is the determined area of the reconstructed capillary at position2 and $A_{solid,2}$ is the determined area of the resolidified area, marked by the yellow dashed line in Fig. 3. For every other position between position 1 and the end of the capillary, the liquid area can be determined as described above.

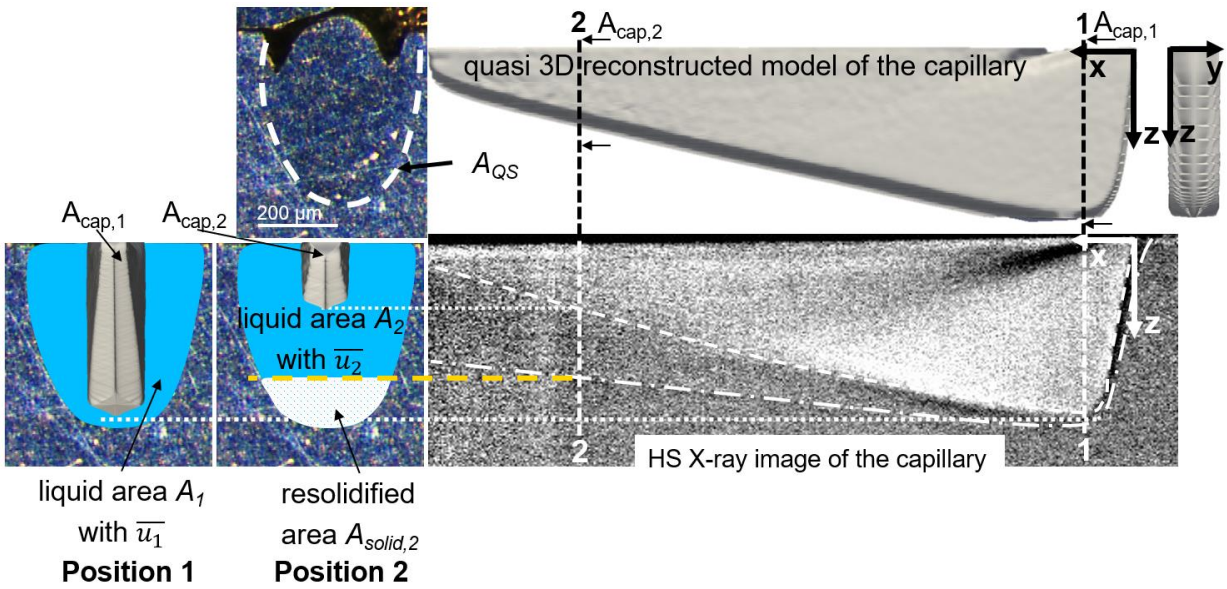

Fig. 3. HS- X-ray image of the wedge-shaped capillary (2 m/s, 2.8 kW) and the quasi 3D reconstructed capillary of the X-ray image of the capillary. Position 1 and 2 are indicated by the dashed line. The measured area A_{QS} of the cross section is marked in the cross section. The determined liquid area for the two positions, A_1 and A_2 are marked by the blue area in the picture on the left.

The volume flow $\dot{V}$ was calculated with

$$\dot{V} = A_{QS} \cdot v \tag{3}$$

It was assumed that the volume flow was constant over the time. Losses such as friction were neglected. Following the average melt velocities $\bar{u}$ at the position 1 and 2 were determined with

$$\overline{u_1} = \frac{\dot{V}}{A_1} \text{ and } \overline{u_2} = \frac{\dot{V}}{A_2} \tag{4}$$

using the results of equation (3) and (1) at position 1 and the results of equation (2) for position 2 respectively. For wedge-shaped capillary, shown in Fig. 3, the determined average melt velocity at position 1 was $\overline{u_1} = 4.2\ \frac{\mathrm{m}}{\mathrm{s}}$ and at position 2 it was $\overline{u_2} = 2.3\ \frac{\mathrm{m}}{\mathrm{s}}$. The average melt velocity deviation $\frac{du}{dt}$ between position1 and the end of the capillary for the wedge-shaped can be calculated with

$$\frac{du}{dt} = \frac{\dot{V}}{\frac{dA}{dt}}. \tag{5}$$

Since no losses such as friction or heat losses were considered in that estimation, the absolute average melt deviation was probably even higher. It is important to keep in mind that the determined average melt velocity $\bar{u}$ is only an average value for one cross section area. There were probably high velocity gradients in the area itself which are not represented by the average melt velocity. For instance, the melt velocity on the surface of the sample in A_1 was probably higher than the melt velocity at the bottom of the capillary. The maximum melt velocity u_{max} on the surface of the sample in A_1 can be calculated with Beck, 1996

$$u_{max} = v[1 + 2\sqrt{\frac{1}{5}\left(\frac{T_V + T_{m-2}T_0}{T_V - T_m}\right)^{\frac{5}{4}}\left(\frac{2\kappa}{v * r_{cap}}\right)^{-3/4}} \quad (6)$$

where T_V is evaporation temperature, T_m is the melting temperature, T_o is the ambient temperature and κ the thermal diffusivity $\kappa = \frac{\lambda}{\rho\, c_p}$ with the density ρ, the specific heat capacity c_p and the thermal conductivity λ. The comparison of u_{max} and the determined average melt velocity $\overline{u_1}$ in A_1 at position 1 for different feed rates v are shown in Fig. 4. The graph shows on the abscissa the feed rate and the melt velocity on the ordinate. The melt velocity increases linearly for increasing feed rates and the average melt velocity is approximately three times as high as the feed rate. It can be seen, that the determined average melt velocity $\overline{u_1}$ is smaller than the calculated u_{max}. Additionally, it can be seen that for increasing feed rates the difference between the determined average melt velocity $\overline{u_1}$ and the calculated u_{max} increases. The error bars indicate the error caused by the measuring inaccuracy of the cross sections and of the inaccuracy of the reconstructed capillaries.

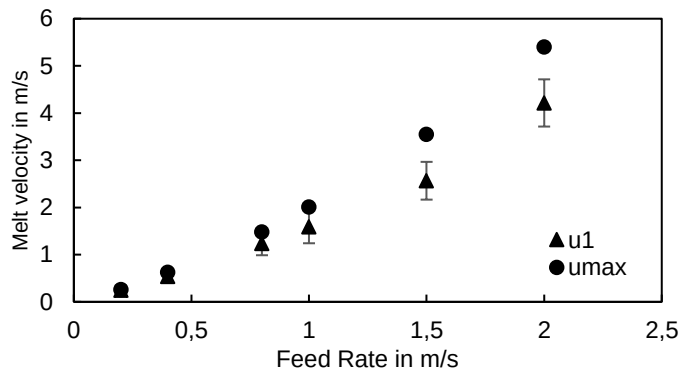

Fig. 4. Determined average melt velocity u_1 and calculated u_{max} for different feed rates.

4. Conclusion

Synchrotron high-speed X-ray images at high feed rates up to 2 m/s were presented in this paper. For the first time, the flow inside the weld pool was analyzed for high feed rates. A new method was proposed to derive the average melt velocity $\overline{u_1}$ in the weld pool in a cross section where the capillary is the deepest. Although no losses and only the average velocities were considered. The results agree very well with the maximum values determined in literature. It was also shown that the melt velocity increases linearly for increasing feed rates of up to 2 m/s and the average melt velocity was approximately three times as high as the feed rate.

Acknowledgements

This research was supported by Trumpf GmbH & Co. KG. The presented investigations were carried out in cooperation with DESY in Hamburg and with RWTH Aachen University within the framework of the Collaborative Research Centre SFB1120-236616214 “Bauteilpräzision durch Beherrschung von Schmelze und Erstarrung in Produktionsprozessen” and funded by the Deutsche Forschungsgemeinschaft e.V. (DFG, German Research Foundation). We acknowledge DESY (Hamburg, Germany), a member of the Helmholtz Association HGF, for the provision of experimental facilities. Parts of this research were carried out at PETRA III and we

would like to thank F. Beckmann and J. Moosmann for assistance in using P07 EH4. Beamtime was allocated for proposal I-20191140.The sponsorship and support is gratefully acknowledged. The presented work was funded by DFG „Modellierung der Kapillare beim Lasertiefschweißen mit der Smoothed Particle Hydrodynamics Methode“ 266218804.

References

Beck M. (1996). Modellierung des Lasertiefschweißens, 1st edn. Vieweg + Teubner, Stuttgart

Boley M., Abt F., Weber R., Graf T., 2013. X-Ray and Optical Videography for 3D Measurement of Capillary and Melt Pool Geometry in Laser Welding. Physics Procedia 41, pp 488–495. doi: 10.1016/j.phpro.2013.03.105

Fabbro R., 2010. Melt pool and keyhole behaviour analysis for deep penetration laser welding. J. Phys. D: Appl. Phys. 43, p 445501. doi: 10.1088/0022-3727/43/44/445501

Fetzer F., Hagenlocher C., Weber R., Graf T., 2021. Geometry and stability of the capillary during deep-penetration laser welding of AlMgSi at high feed rates. Optics & Laser Technology 133, p 106562. doi: 10.1016/j.optlastec.2020.106562

Hagenlocher C., Fetzer F., Weber R., Graf T., 2018. Benefits of very high feed rates for laser beam welding of AlMgSi aluminum alloys. Journal of Laser Applications 30, p 12015. doi: 10.2351/1.5003795

Kouraytem N., Li X., Cunningham R., Zhao C., Parab N., Sun T., Rollett A. D., Spear A. D., Tan W., 2019. Effect of Laser-Matter Interaction on Molten Pool Flow and Keyhole Dynamics. Phys. Rev. Applied 11. doi: 10.1103/PhysRevApplied.11.064054

Lind J., Hagenlocher C., Blazquez-Sanchez D., Hummel M., Olowinsky A., Weber R., Graf T. Influence of the laser cutting front geometry on the striation formation analysed with high-speed synchrotron X-ray imaging. In: Proceedings of NoLamp 2021

Schell N., King A., Beckmann F., Fischer T., Müller M., Schreyer A., 2013. The High Energy Materials Science Beamline (HEMS) at PETRA III. Mechanical Stress Evaluation by Neutrons and Synchrotron Radiation VI 772, pp 57–61. doi: 10.4028/www.scientific.net/MSF.772.57